Nanostructures

DOI: 10.1002/anie.201203347

Morphology- and Phase-Controlled Iron Oxide Nanoparticles Stabilized with Maleic Anhydride Grafted Polypropylene**

Qingliang He, Tingting Yuan, Suying Wei, Neel Haldolaarachchige, Zhiping Luo, David P. Young, Airat Khasanov, and Zhanhu Guo**

Magnetic nanoparticles (NPs) with different morphologies including nanowires and hollow nanospheres have potential applications in energy storage, catalysis, nanoelectronics, and electromagnetic devices.[1] Magnetic iron oxide (Fe_2O_3) NPs have been synthesized by numerous chemical approaches,[1c–g,2] and the typical thermal decomposition methods involve metal precursors like $Fe(CO)_5$ and low-molecular-weight surfactants in solution. Uniform nanocrystals having a controlled size and shape can be achieved by using fatty acid surfactants such as oleic acid and lauric acid, and amines like oleylamine and trioctylamine;[1c,f,2a,3] however, the resulting NPs have poor compatibility with a variety of polyolefins. The production of NPs capable of hosting an inert polyolefin is a prerequisite for the preparation of polyolefin nanocomposites with multiple functionalities.

In nature Fe_2O_3 occurs in two stable crystalline phases (α, and γ), which differ significantly in their geometric structures and magnetic properties.[4] At room temperature, α-Fe_2O_3 behaves as a weak ferromagnet or a canted antiferromagnet, while γ-Fe_2O_3 is a typical ferromagnetic material. Because of the nontoxicity, abundance, chemical stability, and low cost of iron oxide, γ-Fe_2O_3 is used extensively in magnetic resonance imaging and drug delivery,[4] while α-Fe_2O_3 is a promising photoelectrode material for solar-driven water splitting.[5] γ-Fe_2O_3 is thermodynamically unstable and can be converted to α-Fe_2O_3 at temperatures higher than 350 °C (or even higher if the material is stabilized by a polymer); this threshold value primarily depends on the size and morphology of the material.[4] Meanwhile, the opposite transformation from α- to γ-Fe_2O_3 is also reported to be a high-temperature process.[6] For Fe_2O_3 NPs synthesized from conventional metal–surfactant complexes, it is impossible to transform the crystalline phase (from γ- to α-Fe_2O_3 or vice versa) without damaging the stabilizer because of its reported low decomposition temperature. Thus, the solution synthesis of Fe_2O_3 NPs having controlled crystalline phases is of great interest because it requires far less energy than the solid-state transformation of crystalline phases.

Maleic anhydride grafted polypropylene (PP-g-MA) is commonly used as a compatibilizer between a polymer matrix and fillers like organoclay,[7] double-layered hydroxides,[8] and carbon nanotubes[9] in the fabrication of polymer nanocomposites. The advantages of PP-g-MA are that its PP backbone structure is miscible with polyolefins and its MA functional groups are capable of bonding with many organic and inorganic compounds. However, PP-g-MA has rarely been reported in the synthesis of magnetic NPs.

Herein we report on the synthesis of highly stabilized Fe_2O_3 NPs with tunable morphologies, crystalline structures, and magnetic properties by a facile low-temperature, surfactant-assisted solution-phase reaction, that is, the thermal decomposition of $Fe(CO)_5$ in refluxing PP-g-MA/xylene solution. Specifically, as an alternative to fatty acid and amine surfactants, PP-g-MA ($M_n \approx 8000$; structure shown in Scheme S1 in the Supporting Information) is used to stabilize the in situ formed Fe_2O_3 NPs without any further postexperimental procedures. By controlling the weight ratio of PP-g-MA to $Fe(CO)_5$, we demonstrate for the first time the synthesis of stable 1) monodispersed α-phase superparamagnetic hollow Fe_2O_3 NPs and 2) γ-phase ferromagnetic Fe_2O_3 nanowires.

Agglomerated NPs with large, randomly formed clusters were observed (Figure S1a) following the direct thermal decomposition of $Fe(CO)_5$ in refluxing xylene; this cluster formation is attributed to the magnetic dipole–dipole interactions and van der Waals forces among the NPs.[10] NPs with a network structure were observed (Figure S1b) following the thermal decomposition of $Fe(CO)_5$ in commercial isotactic PP/xylene (weight ratio PP/$Fe(CO)_5$ = 1:3.5, decomposition time: 3 h). Because of the high loading and intrinsic magnetic affinity of NPs, the magnetic dipole forces are stronger than the steric repulsion forces of the polymer chains adsorbed on the NPs, hence leading to aggregates of the as-prepared NPs.

[*] Q. He, Dr. T. Yuan, Prof. Dr. Z. Guo
Department of Chemical Engineering, Lamar University
4400 South Martin Luther King Junior Parkway, Beaumont, TX 77705 (USA)
E-mail: zhanhu.guo@lamar.edu
Homepage: http://dept.lamar.edu/zhanhu/icl/
Prof. Dr. S. Wei
Department of Chemistry and Biochemistry, Lamar University
Beaumont, TX 77705 (USA)
E-mail: suying.wei@lamar.edu
Dr. Z. Luo
Microscopy and Imaging Center
Materials Science and Engineering Program
Texas A&M University, College Station, TX 77843 (USA)
N. Haldolaarachchige, Prof. Dr. D. P. Young
Department of Physics and Astronomy
Louisiana State University, Baton Rouge, LA 70803 (USA)
Dr. A. Khasanov
Department of Chemistry
University of North Carolina at Asheville
Asheville, NC 28804 (USA)

[**] This project was financially supported by NSF CBET 11-37441.
Supporting information for this article is available on the WWW under http://dx.doi.org/10.1002/anie.201203347.

Monodispersed NPs with a diameter of (7.7 ± 1.0) nm formed (Figure 1a) when a PP-g-MA/xylene solution was heated at reflux (weight ratio PP-g-MA/$Fe(CO)_5 = 1{:}3.5$, decomposition time: 3 h). Interestingly, the high-resolution (HR) TEM image shows a hollow structure of the as-prepared

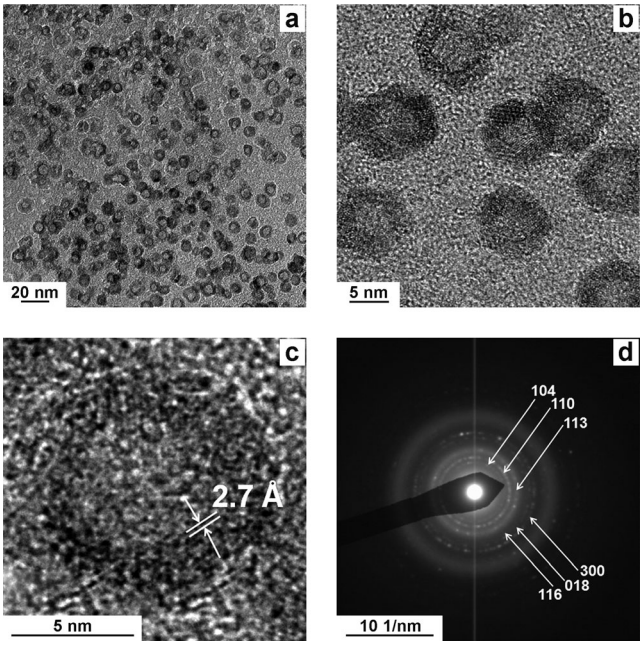

Figure 1. Hollow Fe_2O_3 NPs formed in PP-g-MA/xylene solution: a) low-magnification TEM image, b) HRTEM image, c) HRTEM image of a single hollow particle, and d) SAED pattern. Synthesis conditions: 1.0 g PP-g-MA, 3.5 g $Fe(CO)_5$, 3 h thermal decomposition under air.

NPs in which the hollow core has a diameter of approximately 6 nm and the shell is roughly 1 nm thick (Figure 1b). Moreover, the measured 2.7 Å lattice fringe (Figure 1c) corresponds to the (104) plane of α-phase Fe_2O_3 (PDF no. 33-0664). Upon further investigation of the selected-area electron diffraction (SAED) pattern, the assigned (104), (110), (113), (116), (018), and (300) diffraction planes were found to correspond to α-Fe_2O_3 (PDF no. 33-0664) (Figure 1d). In addition, the low-magnification SEM image reveals that the PP-g-MA nanocomposites have a uniform intumescent porous structure (Figure S2a), while the high-magnification SEM image shows well-dispersed spherical NPs in the PP-g-MA matrix (Figure S2b).

When the weight ratio of PP-g-MA to Fe was changed (PP-g-MA/$Fe(CO)_5 = 0.25{:}3.5$), the formed colloids cast on the surface of a copper grid were observed to be assembled into extended nanowires several micrometers in length (Figure 2a). The HRTEM image shows core–shell NPs with an average diameter of about 20.0 nm (Figure 2b,c). The measured 2.08 Å lattice fringe (Figure 2c) corresponds to the (400) plane of γ-Fe_2O_3 (PDF no. 39-1346). Moreover, the assigned (220), (311), (400), and (440) diffraction planes from the SAED pattern (Figure 2d) correspond to γ-Fe_2O_3 (PDF no. 39-1346). It is worth noting that the SEM image shows highly entangled nanowires (Figure S3), indicating that the

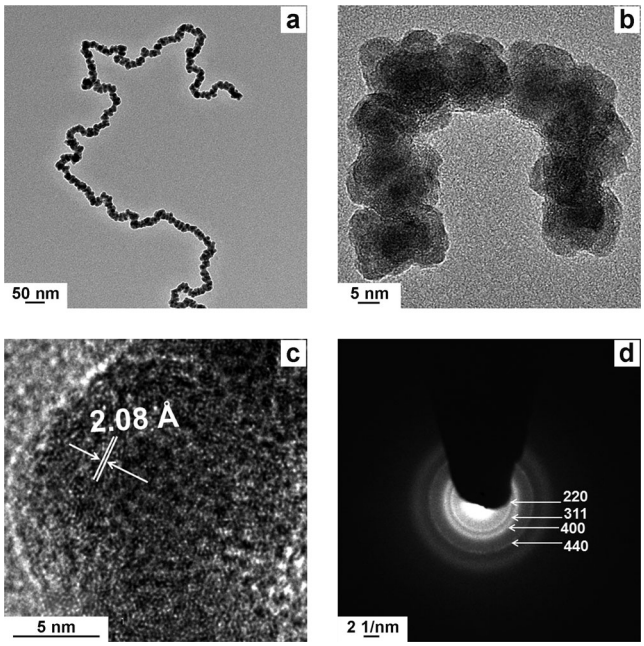

Figure 2. Fe_2O_3 nanowires formed in PP-g-MA/xylene solution: a) low-magnification TEM image, b) HRTEM image, c) HRTEM image of a single particle, and d) SAED pattern. Synthesis conditions: 0.25 g PP-g-MA, 3.5 g $Fe(CO)_5$, 3 h thermal decomposition under air.

wire structure remains intact during the formation of nanocomposites when the colloids are dried.

In room-temperature magnetic measurements, the PP-g-MA nanocomposites with hollow Fe_2O_3 NPs did not reach a saturation value even at an applied field of 30 kOe (Figure S4) and the extrapolated saturation magnetization (M_s) is 2.9 emu g^{-1} (Figure 3a), which is characteristic of α-Fe_2O_3.[11] Moreover, no magnetic hysteresis loop is observed, indicating superparamagnetic behavior for the hollow α-Fe_2O_3 NPs (Figure S4). However, a clear magnetic hysteresis loop with a strong M_s value of 54.0 emu g^{-1} (Figure 3b) and coercivity (H_c) of 518.0 Oe is observed, indicating that the PP-g-MA/Fe_2O_3 (nanowire) composite displays hard ferromagnetic behavior. (Materials with H_c values greater than 200 Oe

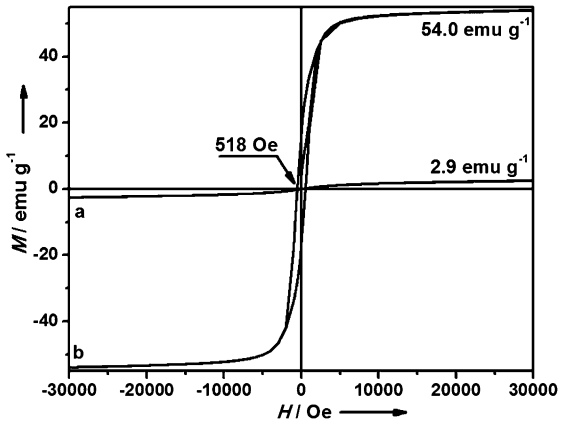

Figure 3. Room-temperature hysteresis loops of the PP-g-MA nanocomposites with a) hollow Fe_2O_3 NPs and b) Fe_2O_3 nanowires.

are defined as hard ferromagnetic, those with H_c values smaller than 200 Oe are referred to as soft ferromagnetic.)

Room-temperature ^{57}Fe Mössbauer spectra were analyzed to further confirm both species, hollow NPs and nanowires. For the hollow NPs, an isomer shift (IS) of 0.35 mm s^{-1} and a quadrupole splitting (QS) of 0.94 mm s^{-1} were observed, indicating pure Fe^{3+}, in other words, Fe_2O_3 in a distorted environment[12] (Figure S5a). The doublet indicates that the α-Fe_2O_3 NPs are superparamagnetic,[13] which is consistent with the lack of a magnetic hysteresis loop (Figure S4). For the nanowires, the ^{57}Fe Mössbauer spectrum (Figure S5b) also shows only one component at IS = 0.35 mm s^{-1}, QS = 0.55 mm s^{-1}, and H_c = 274 kOe. The value of the hyperfine field cannot be used to identify the phase; however, the IS is characteristic of Fe^{3+},[13] indicating that the wires are also pure Fe^{3+}. Thermal gravimetric analysis (Figure S6) indicates a particle loading of 67.2 wt % in the PP-g-MA/γ-Fe_2O_3 nanocomposites. The M_s value of bulk γ-Fe_2O_3 is about 80 emu g^{-1}.[14] It can be deduced that the M_s value of 54.0 emu g^{-1} is completely attributed to γ-Fe_2O_3, which further confirms that the Fe_2O_3 nanowires are in the γ phase.

The X-ray photoelectron spectra (XPS) (Fe 2p) of the hollow NPs depict two intensive peaks at Fe $2p_{3/2}$ (709.0 eV) and Fe $2p_{1/2}$ (722.1 eV) each with a satellite peak, which is in good agreement with the previously reported spectra of α-Fe_2O_3 (Figure S7a).[11a] Meanwhile, the XPS Fe 2p spectra of the wires show two intensive peaks at Fe $2p_{3/2}$ (709.6 eV) and Fe $2p_{1/2}$ (722.7 eV) with only one satellite peak around Fe $2p_{1/2}$ (Figure S7b), which shows good agreement with the reported spectra of γ-Fe_2O_3.[15]

The mechanisms for the formation of hollow Fe_2O_3 NPs and Fe_2O_3 nanowires can be explained by the Kirkendall effect and assembly effects induced by magnetic dipole–dipole interactions, respectively. The synthesis of nanometer-sized hollow CoO and Co_3O_4, Fe_3O_4, Ni/NiO, FePt@Fe_3O_4, and Ag/Fe_2O_3 NPs has been interpreted based on the Kirkendall effect.[1a,d,16] In a unary metal system, the Kirkendall effect refers to a preferred outward diffusion of metal atoms leading to a net material flux across the spherical interface and the consequent formation of a single void at the center.[16a,17] Here, the formation of hollow Fe_2O_3 NPs is also attributed to the nano-scale Kirkendall effect. Specifically, metallic iron nuclei formed in hot solution upon the decomposition of $Fe(CO)_5$, and then oxidized under air such that the Fe NP surface was covered with an oxide layer (Figure S8). The MA functional groups are hydrolyzed into carboxylate groups and bound on the oxide layer (refer to XPS spectra in Figure S9 and the explanation in the Supporting Information). Meanwhile, the adsorbed PP backbone on the NPs restricts the growth of Fe NPs to a final average diameter of roughly 8 nm. At extended reaction times, the outward diffusion of Fe through the oxide layer becomes faster than the inward diffusion of oxygen; the Fe core is gradually consumed and the core shrinks, resulting in the formation of core–shell–void intermediate structures (Figure 4). The TEM image also shows an Fe bridge between a core and a shell, which is similar to what has been observed in the synthesis of hollow Co-S[16a] and Fe-Fe_3O_4[1d] NP systems. The existing bridge provides a fast transport path for the outward diffusion of Fe atoms and stays connected to the shell until the core is completely depleted. Finally, after constant heating for 3 hours with exposure to air, the hollow Fe_2O_3 NPs are formed with total consumption of the Fe core (Figure 1 b).[1d,16a] Scheme S2 depicts the evolution of these hollow Fe_2O_3 NPs.

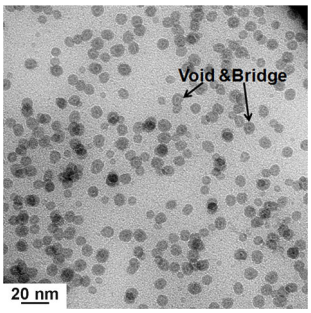

Figure 4. TEM image of intermediate structures in the formation of hollow Fe_2O_3 NPs in PP-g-MA/xylene solution: NPs with core–shell–void structures. Conditions: 2 h thermal decomposition under air.

When we changed the PP-g-MA/$Fe(CO)_5$ weight ratio (here we decreased the amount of PP-g-MA in order to increase the relative Fe loading), the as-prepared Fe_2O_3 NPs became larger with an average size of 20 nm and the bonded PP-g-MA chains restricted the aggregation of NPs to some extent. However, the repulsive forces from short PP-g-MA chains were not strong enough to completely separate these NPs. Hence, Fe_2O_3 nanowires formed by self-assembly through the effects of magnetic dipole–dipole interactions and weak van der Waals forces between the surrounding PP-g-MA molecules (Scheme S3); this was also observed in Co and Co-Se NPs.[18]

In summary, we have described a new facile one-pot strategy to prepare α- and γ-Fe_2O_3 NPs using PP-g-MA as an alternative surfactant. MA served as the surfactant and PP chains served as the hosting matrix to stabilize the in situ formed Fe_2O_3 NPs. The advantage of PP-g-MA also includes its good compatibility with many kinds of polymers. By controlling the PP-g-MA/$Fe(CO)_5$ weight ratio, we could synthesize approximately 7.7 nm diameter superparamagnetic hollow α-Fe_2O_3 NPs and 20.0 nm diameter ferromagnetic γ-Fe_2O_3 nanowires with a coercivity of 518 Oe at moderate temperatures (≈140 °C) in solution for the first time. With a large specific surface area and low density, the as-synthesized hollow α-Fe_2O_3 NPs can be utilized to fabricate lightweight structural materials and for catalysis, nanoelectronics, and drug-delivery applications.[1d,19] Meanwhile, the ferromagnetic γ-Fe_2O_3 nanowires with such high magnetic coercitiy can be applicable as a magnetic storage medium.[20] PP-g-MA can be used to produce other transition-metal-oxide NPs which are currently being explored to prepare hollow NPs and nanowires with controlled density and conductivity for applications in magnetic storage, microwave absorption, and high-frequency electromagnetic interference shielding devices.

Experimental Section

The synthesis of hollow Fe_2O_3 NPs: First, PP-g-MA (1.0 g) and xylene (100 mL) were loaded into a 250 mL three-neck flask and heated to reflux then maintaining refluxing for 30 min to completely dissolve PP-g-MA. Second, $Fe(CO)_5$ (3.5 g) was injected into the hot solution, and the solution immediately became yellow. Finally, the reaction mixture became a black colloidal mixture upon refluxing for 3 h. After cooling to room temperature, the black solution was poured onto a large glass container so that xylene could evaporate in the fume hood. Then the remaining black powder was dried in a vacuum oven for 24 h to form the final composites. For further information about other detailed experimental synthesis and additional information on TEM, SEM, XPS, TGA, and magnetic properties, see the Supporting Information.

Received: May 1, 2012
Published online: July 31, 2012

Keywords: iron oxide · Kirkendall effect · nanoparticles · nanowires

[1] a) P. Y. Keng, B. Y. Kim, I. B. Shim, R. Sahoo, P. E. Veneman, N. R. Armstrong, H. Yoo, J. E. Pemberton, M. M. Bull, J. J. Griebel, *ACS Nano* **2009**, *3*, 3143 – 3157; b) P. Sudeep, T. Emrick, *ACS Nano* **2009**, *3*, 2870 – 2875; c) S. Peng, C. Wang, J. Xie, S. Sun, *J. Am. Chem. Soc.* **2006**, *128*, 10676 – 10677; d) S. Peng, S. Sun, *Angew. Chem.* **2007**, *119*, 4233 – 4236; *Angew. Chem. Int. Ed.* **2007**, *46*, 4155 – 4158; e) U. Jeong, X. Teng, Y. Wang, H. Yang, Y. Xia, *Adv. Mater.* **2007**, *19*, 33 – 60; f) J. Park, J. Joo, S. G. Kwon, Y. Jang, T. Hyeon, *Angew. Chem.* **2007**, *119*, 4714 – 4745; *Angew. Chem. Int. Ed.* **2007**, *46*, 4630 – 4660.

[2] a) T. Hyeon, S. S. Lee, J. Park, Y. Chung, H. B. Na, *J. Am. Chem. Soc.* **2001**, *123*, 12798 – 12801; b) S. Santra, R. Tapec, N. Theodoropoulou, J. Dobson, A. Hebard, W. Tan, *Langmuir* **2001**, *17*, 2900 – 2906; c) C. E. Bunker, J. J. Karnes, *J. Am. Chem. Soc.* **2004**, *126*, 10852 – 10853; d) A. Prakash, A. V. McCormick, M. R. Zachariah, *Chem. Mater.* **2004**, *16*, 1466 – 1471; e) M. F. Casula, Y. Jun, D. J. Zaziski, E. M. Chan, A. Corrias, A. P. Alivisatos, *J. Am. Chem. Soc.* **2006**, *128*, 1675 – 1682; f) J. F. Berret, N. Schonbeck, F. Gazeau, D. El Kharrat, O. Sandre, A. Vacher, M. Airiau, *J. Am. Chem. Soc.* **2006**, *128*, 1755 – 1761; g) A. Cabot, V. F. Puntes, E. Shevchenko, Y. Yin, L. Balcells, M. A. Marcus, S. M. Hughes, A. P. Alivisatos, *J. Am. Chem. Soc.* **2007**, *129*, 10358 – 10360; h) C. Kaittanis, S. Santra, J. M. Perez, *J. Am. Chem. Soc.* **2009**, *131*, 12780 – 12791; i) C. J. Jia, L. D. Sun, F. Luo, X. D. Han, L. J. Heyderman, Z. G. Yan, C. H. Yan, K. Zheng, Z. Zhang, M. Takano, *J. Am. Chem. Soc.* **2008**, *130*, 16968 – 16977; j) E. Valero, S. Tambalo, P. Marzola, M. Ortega-Muñoz, F. J. López-Jaramillo, F. Santoyo-González, J. de Dios López, J. J. Delgado, J. J. Calvino, R. Cuesta, *J. Am. Chem. Soc.* **2011**, *133*, 4889 – 4895; k) S. Laurent, D. Forge, M. Port, A. Roch, C. Robic, L. Vander Elst, R. N. Muller, *Chem. Rev.* **2008**, *108*, 2064 – 2110.

[3] a) K. Woo, J. Hong, S. Choi, H. W. Lee, J. P. Ahn, C. S. Kim, S. W. Lee, *Chem. Mater.* **2004**, *16*, 2814 – 2818; b) F. X. Redl, T. Charles, G. C. Papaefthymiou, R. L. Sandstrom, M. Yin, H. Zeng, C. B. Murray, S. P. O'Brien, *J. Am. Chem. Soc.* **2004**, *126*, 14583 – 14599; c) H. Kim, M. Lee, Y. Kim, J. Huh, M. Kim, T. Kim, V. N. Phan, Y. B. Lee, G. R. Yi, *Angew. Chem.* **2009**, *121*, 5231 – 5235; *Angew. Chem. Int. Ed.* **2009**, *48*, 5129 – 5133.

[4] L. Machala, J. Tuček, R. Zbor?il, *Chem. Mater.* **2011**, *23*, 3255 – 3272.

[5] Y. Ling, G. Wang, J. Reddy, C. Wang, J. Z. Zhang, Y. Li, *Angew. Chem.* **2012**, *124*, 4150 – 4155; *Angew. Chem. Int. Ed.* **2012**, *51*, 4074 – 4079.

[6] a) F. Jiao, J. C. Jumas, M. Womes, A. V. Chadwick, A. Harrison, P. G. Bruce, *J. Am. Chem. Soc.* **2006**, *128*, 12905 – 12909; b) Q. Han, Z. Liu, Y. Xu, Z. Chen, T. Wang, H. Zhang, *J. Phys. Chem. C* **2007**, *111*, 5034 – 5038.

[7] S. Morlat, B. Mailhot, D. Gonzalez, J. L. Gardette, *Chem. Mater.* **2004**, *16*, 377 – 383.

[8] P. J. Purohit, J. E. Huacuja-Sánchez, D. Y. Wang, F. Emmerling, A. Thünemann, G. Heinrich, A. Schönhals, *Macromolecules* **2011**, *44*, 4342 – 4354.

[9] M. C. Hsiao, S. H. Liao, Y. F. Lin, C. C. Weng, H. M. Tsai, C. C. M. Ma, S. H. Lee, M. Y. Yen, P. I. Liu, *Energy Environ. Sci.* **2011**, *4*, 543 – 550.

[10] M. Yoonessi, J. A. Peck, J. L. Bail, R. B. Rogers, B. A. Lerch, M. A. Meador, *ACS Appl. Mater. Interfaces* **2011**, *3*, 2686 – 2693.

[11] a) X. Qu, N. Kobayashi, T. Komatsu, *ACS Nano* **2010**, *4*, 1732 – 1738; b) S. Zeng, K. Tang, T. Li, Z. Liang, D. Wang, Y. Wang, Y. Qi, W. Zhou, *J. Phys. Chem. C* **2008**, *112*, 4836 – 4843; c) K. T. Van, H. G. Cha, K. C. Nguyen, S. W. Kim, M. H. Jung, Y. S. Kang, *Cryst. Growth Des.* **2012**, *12*, 862 – 868.

[12] S. Hanna, *Science* **1969**, *164*, 939 – 939.

[13] E. Kuzmann, S. Nagy, A. Vertes, *Pure Appl. Chem.* **2003**, *75*, 801 – 858.

[14] P. Dutta, A. Manivannan, M. Seehra, N. Shah, G. Huffman, *Phys. Rev. B* **2004**, *70*, 174428.

[15] a) J. Lu, X. Jiao, D. Chen, W. Li, *J. Phys. Chem. C* **2009**, *113*, 4012 – 4017; b) I. T. Kim, G. A. Nunnery, K. Jacob, J. Schwartz, X. Liu, R. Tannenbaum, *J. Phys. Chem. C* **2010**, *114*, 6944 – 6951.

[16] a) Y. Yin, R. M. Rioux, C. K. Erdonmez, S. Hughes, G. A. Somorjai, A. P. Alivisatos, *Science* **2004**, *304*, 711 – 714; b) J. G. Railsback, A. C. Johnston-Peck, J. Wang, J. B. Tracy, *ACS Nano* **2010**, *4*, 1913 – 1920; c) J. Gao, G. Liang, J. S. Cheung, Y. Pan, Y. Kuang, F. Zhao, B. Zhang, X. Zhang, E. X. Wu, B. Xu, *J. Am. Chem. Soc.* **2008**, *130*, 11828 – 11833; d) Y. Pan, J. Gao, B. Zhang, X. Zhang, B. Xu, *Langmuir* **2010**, *26*, 4184 – 4187.

[17] a) K. Tu, U. Gösele, *Appl. Phys. Lett.* **2005**, *86*, 093111; b) H. J. Fan, U. Gösele, M. Zacharias, *Small* **2007**, *3*, 1660 – 1671.

[18] a) P. Y. Keng, I. Shim, B. D. Korth, J. F. Douglas, J. Pyun, *ACS Nano* **2007**, *1*, 279 – 292; b) J. Gao, B. Zhang, X. Zhang, B. Xu, *Angew. Chem.* **2006**, *118*, 1242 – 1245; *Angew. Chem. Int. Ed.* **2006**, *45*, 1220 – 1223.

[19] S. H. Im, U. Jeong, Y. Xia, *Nat. Mater.* **2005**, *4*, 671 – 675.

[20] D. V. Talapin, J. S. Lee, M. V. Kovalenko, E. V. Shevchenko, *Chem. Rev.* **2010**, *110*, 389 – 458.

